17.2 A 28GHz Magnetic-Free Non-Reciprocal Passive CMOS Circulator Based on Spatio-Temporal Conductance Modulation

Tolga Dinc, Harish Krishnaswamy

Columbia University, New York, NY

A significant challenge for silicon-based mm-wave systems is a low-loss shared-antenna (ANT) interface with high linearity, isolation (ISO) and bandwidth (BW). Shared ANT interfaces with simultaneous transmit and receive capability are critical for mm-wave 5G base stations that need to simultaneously communicate with multiple users, FMCW-based radars, and emerging full-duplex systems [1].

Lorentz reciprocity is a fundamental property of any linear and time-invariant medium characterized by symmetric permittivity and permeability tensors. A three-port passive network cannot be reciprocal, lossless, and matched at all ports at the same time. As a result, a reciprocal, passive, matched shared-ANT interface, such as an electrical-balance duplexer (EBD) [2], has at least a 3dB theoretical loss (typically around 4dB at RF/mm-wave). This theoretical loss can be avoided by breaking Lorentz reciprocity. Conventional non-reciprocal circulators rely on ferromagnetic materials, but they are bulky, expensive, and not compatible with CMOS. Active devices are inherently non-reciprocal, but active circulators are severely limited in their linearity and noise performance [3]. In recent years, there has been progress on achieving non-reciprocity and building circulators without magnetic materials by exploiting time-variance, specifically spatio-temporal permittivity modulation at low-RF frequencies [4,5]. In a circuit implementation, the permittivity modulation is achieved using varactors, and in general has limited modulation index on semiconductor substrates (C_{max}/C_{min} is usually around 2-4), either resulting in large form-factors [4] or high losses [5]. In addition, these techniques are yet to be demonstrated on silicon and are also not suitable for mm-wave due to the poor varactor quality factor. On the other hand, conductivity can be easily modulated on a semiconductor substrate using transistors as passive switches. Conductivity modulation has a very high modulation index (CMOS transistor R_{OFF}/R_{ON} can be as high as 10^3 to 10^5), resulting in small form factor and very low loss as demonstrated in the RF CMOS circulator in [6,7] using an N-path filter-based implementation. However, N-path filters are not amenable to mm-wave due to stringent clocking requirements and transistor parasitics.

We present a near-28GHz fully integrated circulator in 45nm SOI CMOS, demonstrating magnetic-free passive non-reciprocity on silicon at mm-wave. Millimeter-wave operation is enabled by the concept of spatio-temporal conductance modulation, which results in the breaking of phase non-reciprocity. The spatio-temporal conductance modulation features the following advantages over the phase-shifted N-path filter concept of [6,7]: (i) modulation or switching is performed at a frequency much lower than the operation frequency (1/3rd in this case), enabling operation at mm-wave, (ii) four 50% duty-cycle I/Q phases are required, as opposed to a large number of low-duty-cycle clock phases typically used in N-path filters, again easing mm-wave operation, and (iii) switching is performed across transmission-line delays, as opposed to capacitors as in N-path filters, enhancing BW. The 25GHz circulator achieves 3.3/3.2dB TX-to-ANT/ANT-to-RX insertion losses (IL), respectively, 18.3 to 21.2dB of TX-to-RX isolation (ISO) over the 4.6GHz 1dB IL BW, 3.3 to 4.4dB ANT-to-RX NF, and >21dBm TX-to-ANT/ANT-to-RX input P1dB.

The spatio-temporal conductance modulation concept consists of two sets of I/Q switches implemented as Gilbert quads on either end of I/Q transmission line delays (Fig. 17.2.1). The operation of this structure can be explained with a simplified-circuit theoretic mixing analysis. In the forward direction, the first set of I/Q switches commutates the signal at a frequency (ω_m) lower than the operating frequency (ω_{in}), thus creating two mixing products at $\omega_{in}+\omega_m$ and $\omega_{in}-\omega_m$. The mixing products in the I/Q paths experience phase shifts of $-\phi_1$ and $-\phi_2$ at $\omega_{in}-\omega_m$ and $\omega_{in}+\omega_m$, respectively, as they flow through the transmission lines. On the other end, the second set of I/Q switches commutates the mixing products at ω_m but with a staggered phase shift of ϕ, generating mixing products at ω_{in}, $\omega_{in}+2\omega_m$, and $\omega_{in}-2\omega_m$. The signals at $\omega_{in}-2\omega_m$ and $\omega_{in}+2\omega_m$ are 180° out of phase and cancel out. On the other hand, if $2\phi = \phi_1-\phi_2=-\pi$ (or equivalently, $2\omega_m T_d=\pi$, where T_d is the delay of the transmission line), the mixing products at ω_{in} add up constructively into a single signal with perfect lossless transmission and a phase shift of $\phi-\phi_1$, or -90°$-\phi_1$. A similar analysis in the reverse direction shows lossless transmission but a non-reciprocal phase shift of $-\phi-\phi_1$, or +90° $-\phi_1$. In other words, the spatio-temporal modulation network provides a non-reciprocal phase shift with a 180° difference between forward and reverse directions (and lossless reciprocal magnitude response). We choose $\phi_1=(\omega_{in}-\omega_m)T_d=180°$, giving insertion phases of +90° and -90° in the forward and reverse directions, respectively. Combining this equation with $2\omega_m T_d=\pi$, we obtain $\omega_m=\omega_{in}/3$ (i.e. the third subharmonic). A circulator can now be constructed by exploiting constructive and destructive interference between the non-reciprocal phase element and a reciprocal phase element in forward and reverse directions (Fig. 17.2.1). Similar to [6,7], a 3λ/4 transmission-line loop is wrapped around the non-reciprocal phase component so that signals can circulate in only one direction (-270°-90° results in constructive interference in one direction and -270°+90° results in destructive interference in the other). As mentioned, the use of a lower modulation frequency as well as 50% duty-cycle IQ clocks enables operation at mm-waves. Further, the use of transmission lines in both the reciprocal and non-reciprocal paths leads to better frequency-response matching between them, resulting in superior ISO and IL BWs than in [6,7].

Here, for 25GHz operation, $\omega_m=\omega_{in}/3=8.33$GHz. A differential architecture (Fig. 17.2.2) reduces the LO feedthrough and improves power handling. The fully balanced Gilbert quads are designed using 2×16µm/40nm floating-body transistors, improving the power handling further. Artificial transmission lines with inductor Q of 20 are used in the non-reciprocal phase element, which is symmetrically placed between the TX and RX ports so that device parasitics could be absorbed into the λ/8 artificial transmission lines on either side. The LO path consists of fine-phase-tuning varactors, a 2-stage poly-phase filter generating the differential I/Q signals, and self-biased differential inverter chains to generate the 8.33GHz square clocks.

Figures 17.2.3 to 17.2.5 describe the measurements, in which the on-chip baluns are de-embedded through test structures, and a probe, terminated with a broadband 50Ω load, is landed on the third port in each measurement. The small-signal TX-to-ANT and ANT-to-RX ILs are 3.3dB and 3.2dB, respectively, and a broadband TX-to-RX ISO of 18.3 to 21.2dB over 4.6GHz (the 1dB BW of the ILs) is seen, limited by the impedance of the probe and load at the third port (a challenge for all circulators and exacerbated at mm-wave). The TX-to-ANT/ANT-to-RX input P1dBs are >+21.5/+21dBm, respectively (setup limited). The TX-to-ANT and ANT-to-RX IIP3s are ~+20dBm. The noteworthy P1dBs are high relative to the IIP3s due to a graceful large-signal linearity degradation mechanism inherent to the concept that is beyond the scope of this paper. TX-to-RX ISO compresses by 1dB and 3dB at +11.4dBm and +21.45dBm, respectively. This can be partially compensated by an external ANT impedance tuner, which enables a higher initial small-signal ISO of 25dB (still setup limited) and 1dB compression at +12.3dBm. ANT-RX NF is 3.3 to 4.4dB, consistent with the IL and showing negligible degradation due to LO phase noise. When compared with prior art (Fig. 17.2.6), this work is superior to active mm-wave circulators [3] in all metrics (loss, linearity, NF and BW). When compared with a passive EBD [2], this work achieves >1dB overall advantage in the sum of TX-to-ANT and ANT-to-RX ILs while operating at >10× higher frequency, although techniques to improve power handling and integrated tuners/balance networks for ISO are desirable. When compared with the N-path filter-based circulator of [6,7], this work scales to mm-wave and significantly enhances BW. Losses and LO path power can be lowered further with a process with thick upper metals and by using tuned LO buffers, respectively.

Acknowledgments:
We acknowledge the DARPA ACT program and NSF EFMA 1641100 for financial support, and Global Foundries for fabrication donation.

References:

[1] T. Dinc, et al., "A 60GHz CMOS Full-Duplex Transceiver and Link with Polarization-Based Antenna and RF Cancellation," *IEEE JSSC*, vol. 51, no. 5, pp. 1125-1140, May 2016.

[2] B. van Liempd, et. al., "A +70dBm IIP3 Single-Ended Electrical-Balance Duplexer in 0.18µm SOI CMOS," *ISSCC*, pp. 1-3, Feb. 2015.

[3] J.-F. Chang, et. al., "Design and Analysis of 24-GHz Active Isolator and Quasi-Circulator," *IEEE TMTT*, vol. 63, no. 8, pp. 2638-2649, Aug. 2015.

[4] S. Qin, et. al., "Nonreciprocal Components with Distributedly Modulated Capacitors," *IEEE TMTT*, vol. 62, no. 10, pp. 2260-2272, Oct. 2014.

[5] N. Estep, et al., "Magnetless Microwave Circulators Based on Spatiotemporally Modulated Rings of Coupled Resonators," *IEEE TMTT*, vol. 64, no. 2, pp. 502-518, Feb. 2016.

[6] J. Zhou, et al., "Receiver with Integrated Magnetic-free N-Path-Filter-Based Non-Reciprocal Circulator and Baseband Self-Interference Cancellation for Full-Duplex Wireless," *ISSCC,* pp. 178-180, Feb. 2016.

[7] N. Reiskarimian and H. Krishnaswamy, "Magnetic-Free Non-Reciprocity Based on Staggered Commutation," *Nat. Commun.*, vol. 7, no. 4, Apr. 2016.

 978-1-5090-3758-2/17/$31.00

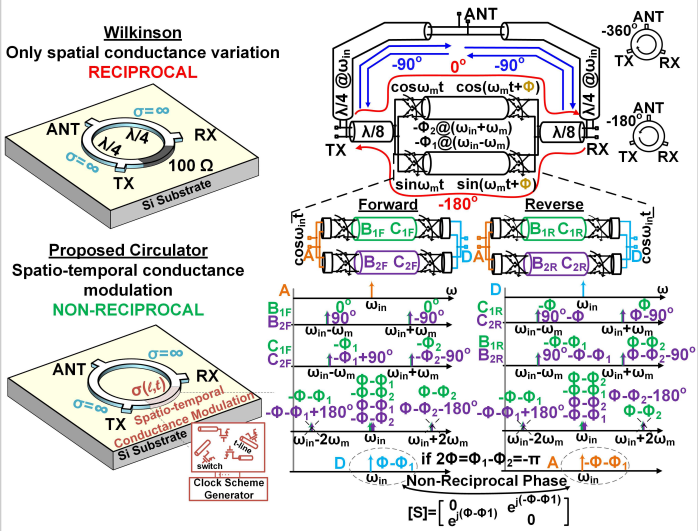

Figure 17.2.1: Magnetic-free non-reciprocal passive mm-wave circulator based on spatio-temporal conductance modulation.

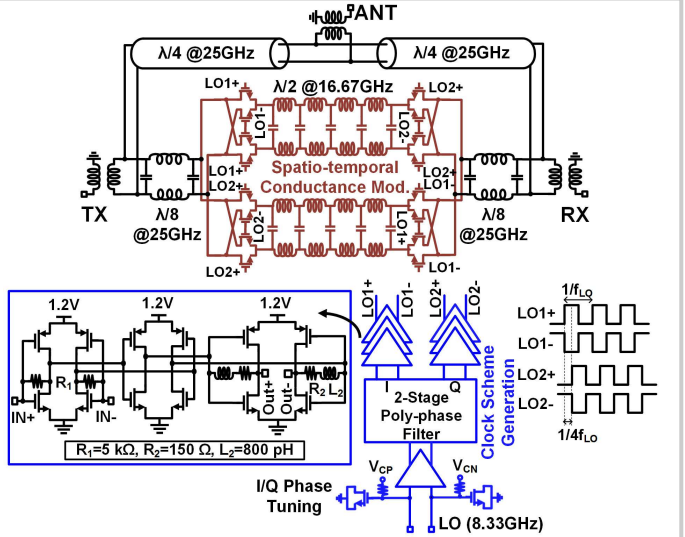

Figure 17.2.2: Block and circuit diagram of the 25GHz magnetic-free non-reciprocal passive 45nm SOI CMOS circulator.

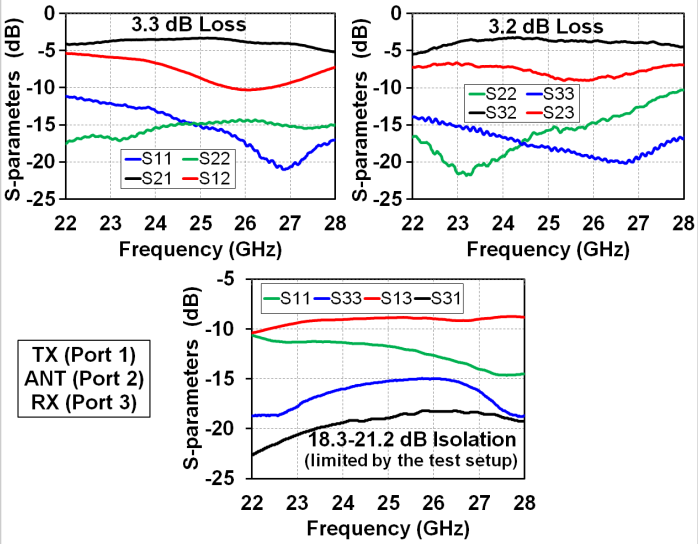

Figure 17.2.3: Measured circulator TX-ANT, ANT-RX and TX-RX S-parameters.

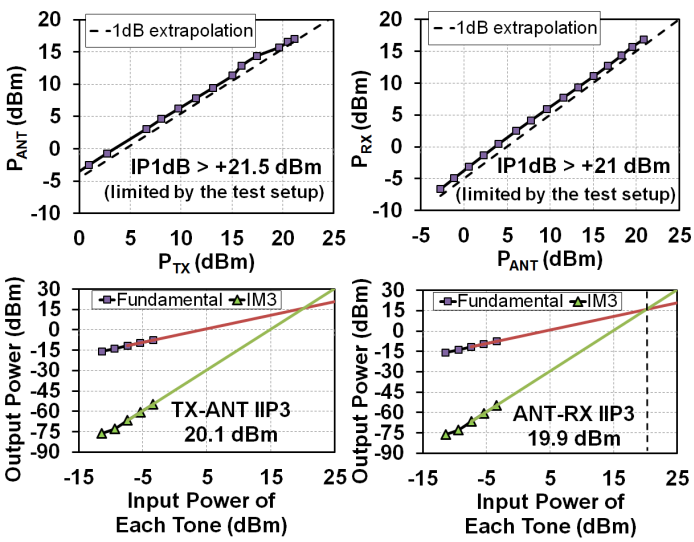

Figure 17.2.4: Circulator TX-ANT and ANT-RX large-signal measurements.

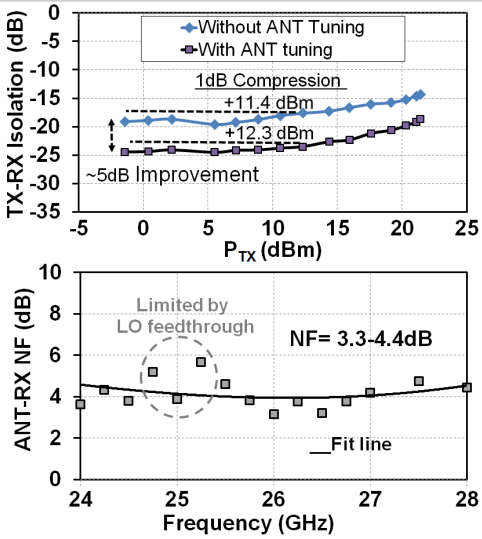

Figure 17.2.5: Measured TX-RX large-signal isolation and circulator ANT-RX noise figure.

	TMTT2010	TMTT2015 [3]	ISSCC2015 [2]	ISSCC2016 [6]	This work
Technique	Active Quasi Circulator	Active Quasi Circulator	Electrical Balance Duplexer	N-Path-Filter-based Magnetic-Free Passive Circulator	Magnetic-Free Passive Circulator Based on Spatio-Temporal Conductance Mod.
Technology	180nm CMOS	180nm CMOS	180nm SOI CMOS	65nm CMOS	**45nm SOI CMOS**
Frequency	24GHz	24GHz	1.9-2.2GHz	0.75GHz	**25GHz**
TX-ANT Transmission	+22.4dB	-5.7dB	-3.7dB	-1.7dB	**-3.3dB**
ANT-RX Transmission	+12.3dB	-5.7dB	-3.9dB	-1.7dB	**-3.2dB**
TX-RX Isolation	>15dB	>20 dB	>40dB	>20dB	**>18.5dB** [4]
Isolation BW [1]	~1%	~1.6%	~15%	4.3%	**18%** [5]
Center frequency/ Modulation frequency	N/A	N/A	N/A	1	**3**
Area	3.22mm²	0.715mm²	1.75mm²	0.64mm²/25mm² [2]	**2.16mm²**
ANT-RX NF	17dB	N/R	3.9dB	4.3dB [3]	**3.3-4.4dB**
TX-ANT IP1dB	-19.8dBm	+9.5dBm	N/R	N/R	**>+21.5dBm**
TX-ANT IIP3	-11dBm	N/R	+70dBm	+27.5dBm	**+19.9dBm**
P_{DC}	144.8mW	7.2mW	0	59mW	**78.4mW**

[1] BW over which an isolation better than the value quoted in the row above is maintained.
[2] Includes SMD inductors on PCB.
[3] Includes 2.3dB degradation due to LO phase noise.
[4] Limited by the mmWave test setup.
[5] This is the 1dB insertion loss BW.
N/A: Not Applicable, N/R: Not Reported

TMTT2010: H. S. Wu, C. W. Wang and C. K. C. Tzuang, "CMOS Active Quasi-Circulator With Dual Transmission Gains Incorporating Feedforward Technique at K-Band," in *IEEE TMTT*, vol. 58, no. 8, pp. 2084-2091, Aug. 2010.

Figure 17.2.6: Performance summary and comparison.

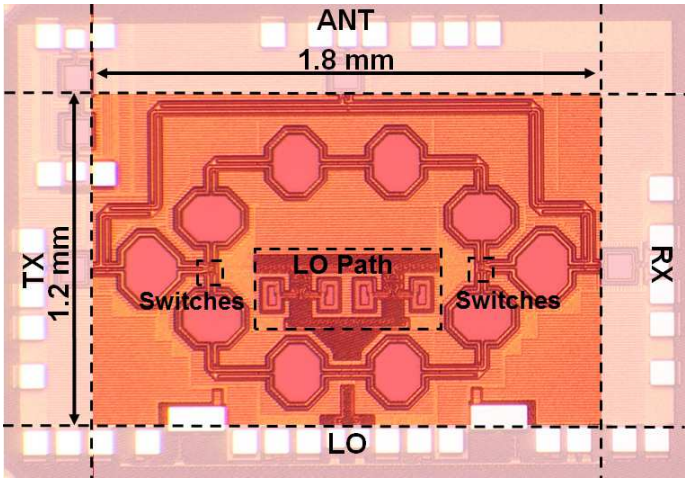

Figure 17.2.7: Die micrograph of the test chip in 45nm SOI CMOS.

978-1-5090-3758-2/17/$31.00